ACCEPTED MANUSCRIPT
Journal of Applied Physics
AIP Publishing
This is the author's peer reviewed, accepted manuscript. However, the online version of record will be different from this version once it has been copyedited and typeset.
PLEASE CITE THIS ARTICLE AS DOI: 10.1063/5.0151255

Elementary Intracellular Ca Signals approximated as a Transition of Release Channel System from a Metastable State

Guillermo Veron[1], Victor A. Maltsev[1], Michael D. Stern[1], Anna V. Maltsev[2]*
[1]Cellular Biophysics Section, Laboratory of Cardiovascular Science,
National Institute on Aging, NIH, Baltimore, MD 21224, USA
[2]School of Mathematical Sciences, Queen Mary University of London, London E14NS, United Kingdom

Keywords:
Calcium spark, ryanodine receptor, excitation-contraction coupling, cardiac arrhythmia

***Author for correspondence:**
Anna V. Maltsev, PhD
Email: a.maltsev@qmul.ac.uk

Abstract
Cardiac muscle contraction is initiated by an elementary Ca signal (called Ca spark) which is achieved by collective action of Ca release channels in a cluster. The mechanism of this synchronization remains uncertain. We approached Ca spark activation as an emergent phenomenon of an interactive system of release channels. We constructed a weakly lumped Markov chain that applies an Ising model formalism to such release channel clusters and probable open channel configurations and demonstrated that spark activation is described as a system transition from a metastable to an absorbing state, analogous to the pressure required to overcome surface tension in bubble formation. This yielded quantitative estimates of the spark generation probability as a function of various system parameters. We performed numerical simulations to find spark probabilities as a function of sarcoplasmic reticulum Ca concentration obtaining similar values for spark activation threshold as our analytic model, as well as those reported in experimental studies. Our parametric sensitivity analyses also showed that the spark activation threshold decreased as Ca sensitivity of RyR activation and RyR cluster size increased.

ACCEPTED MANUSCRIPT

Journal of Applied Physics

AIP Publishing

This is the author's peer reviewed, accepted manuscript. However, the online version of record will be different from this version once it has been copyedited and typeset.
PLEASE CITE THIS ARTICLE AS DOI: 10.1063/5.0151255

1. Introduction

Robust intracellular signals are achieved by synchronous operation of groups of molecules, each operating stochastically. In cardiac muscle, Ca release channels, ryanodine receptors (RyR), form clusters of 20 to 200 channels (Ca release units, CRU) embedded in the sarcoplasmic reticulum (SR). Within CRUs, individual channels are very close to each other (~30 nm) and arranged in an almost perfect rectangular grid. The channels interact via Ca-induced-Ca-release (CICR)[1] thereby facilitating RyR openings throughout the cluster. The all-or-none event when almost all of the channels in a CRU have been opened is referred to as a Ca spark [2]. Ca sparks can be triggered by a Ca influx via L-type Ca channel ("induced sparks"), or arise spontaneously ("spontaneous sparks"). Induced sparks are signals of excitation-contraction coupling in cardiac muscle and spontaneous sparks contribute to normal cardiac impulse initiation in sinoatrial node cells [3]. Ca sparks are also elementary signaling events in skeletal muscle [4] and smooth muscle cells [5, 6]. Networks of beta cell populations generate local Ca signals critical for their function [7]. In neurons high-amplitude local Ca signals, known as puffs, are generated by clusters of IP3 receptors and represent collective events, in which clustered channels are mutually activated also by CICR [8].

Understanding how stochastic transitions of individual molecules are synchronized to generate sparks, puffs and other local signals is an open problem of biological physics and has been the subject of extensive experimental and theoretical research, including multiscale modeling, i.e. bridging scales from individual molecule state transitions to global behavior [9, 10]. Stochastic simulations of the Ca signals have been performed in cardiac cells [11-18] and neurons, [8 19, 20]. In addition to stochastic modeling, another promising approach to the problem is via network science (see recent reviews[10, 21]). Thus, in more general context, clusters of specialized molecules in different cells and tissues synchronize their states to generate the robust elementary intracellular signals over the thermal noise, thus representing the emergence of the first basic level of dynamic signaling essential for life.

Understanding and modeling of local Ca signaling initiation is important for the next scale of events, such as Ca waves. In ventricular myocytes abnormal spontaneous sparks can initiate Ca waves [22] and life-threatening arrhythmia [23]. In sinoatrial cells local Ca releases occurring under normal physiological conditions in the form of relatively small, locally propagating Ca waves contribute to diastolic depolarization, underlying heart automaticity. These local Ca releases have been extensively investigated in individual cells and tissues, including stochastic simulations and multiscale statistical physics approaches [11, 24, 25]. The multiscale modeling, bridging intercellular Ca signaling and Ca waves is an important new approach to assess the origin and velocity of Ca waves in three-dimensions of different biological tissues, e.g. complex dynamic Ca patterns in pancreas tissue slices [26, 27]. In all these circumstances understanding initiation of Ca signals is essential for both basic biophysical research and biomedical applications [28].

Here we study under what conditions RyRs open simultaneously to create a full Ca spark instead of firing individually or with only partial synchronization, all of which have been observed experimentally under various conditions [29]. Zima et al. [30] found that full sparks start forming as the SR Ca load surpasses 300 μM. Despite its fundamental importance, spark activation has not been systematically studied theoretically or numerically as an emergent phenomenon of an interactive system of release channels. Numerical models of the CRU including interacting, stochastically gated RyR channels were reported by Laver et al. [13] and Stern et al. [16], focusing on Ca spark termination. This approach was extended towards

ACCEPTED MANUSCRIPT
Journal of Applied Physics
AIP Publishing
This is the author's peer reviewed, accepted manuscript. However, the online version of record will be different from this version once it has been copyedited and typeset.
PLEASE CITE THIS ARTICLE AS DOI: 10.1063/5.0151255

understanding the effect of different CRU geometries [31]. Other models approximate CRU phenomenologically by a single gating mechanism or as a Markov chain representing a result of interactions of all RyRs within the CRU (the "sticky cluster" model [32]). In 2011, Sato and Bers approximated probabilities of different number of RyRs open in the CRU at a given junctional SR Ca level by using the binomial distribution [33]. This model was further extended to evaluate spark activation probabilities for RyR clusters of different sizes [34]. However, due to the assumption of independence for RyRs inherent in the binomial distribution, this approach lacks the effect of RyR interactions crucial for spark initiation via CICR.

A new approach to describe CRU operation has recently been introduced by the authors in [17], where the Stern model of the CRU [16] was mapped isomorphically to the Ising model. Further analysis identified the critical parameter (referred to as β, similar to inverse temperature) that determines conditions for Ca leak [35]. Both these studies focused again mainly on spark termination. The present study is the first application of the Ising formalism to spark activation.

2. Material and Methods

Here we introduce a new Markov chain describing the numbers of adjacent open channels to explicitly estimate the probability that an open RyR will develop into a spark at each level of SR Ca, thus establishing the threshold SR Ca load at which a spark can occur and offering a mechanistic explanation. Our new approach is that we calculate transition probabilities analytically. However, to compare, we also performed numerical model simulations of spark generation using Stern et al. model [16] in a more recent modification [17]. An important feature of our model is an exponential dependence of open probability on local Ca concentration based on experimental data in Laver et al. [13]. However, this dependence remains controversial due to large variability in channel open times measurements [36-41].

The Stern numerical model of the CRU has been shown to be isomorphic to an Ising model [17], a classical model of statistical physics used to explain spontaneous magnetization. This isomorphism provides a starting point for the present work. The RyRs are assumed to be in a CRU given by a rectangular grid Λ (with their coordinates given as $x = (x_1, x_2)$ and with (0, 0) as the center of a grid with an odd number of elements) with each RyR assuming one of two states: open (+1) or closed (-1). An assignment σ of an open or closed state to each RyR is called a configuration, and the Ising model is a continuous time Markov chain with RyR configurations as states. We notice that σ can be thought of as a matrix, while $\sigma(x)$ is the +1 or -1 state of the CRU placed at position x (see [42] for further explanation of this notation.) The instantaneous transition rates are only non-zero between configurations differing at only one RyR, say at position x, and, upon discretizing time, are given by Eq.6 in [17], which we give here for convenience:

$$P(\sigma,\sigma^x)=\begin{cases}\Delta t C e^{2\beta\left(\sum_{y\in\Lambda_b}\phi(|x-y|)\sigma(y)+h\right)} & \text{for } \sigma(x)=-1\\ \Delta t C & \text{for } \sigma(x)=1\end{cases} \quad (1)$$

Here σ^x is the configuration that coincides with configuration σ except at x where the state is reversed and, for any real number r, $\phi(r)$ is the interaction profile (defined below). Here we embed the grid Λ in a larger grid Λ_b (here the b stands for boundary) where the configuration of boundary RyRs is taken to be always closed (see Supplementary text or [17] for further details). This is to include Ca diffusion out of the CRU in the model.

ACCEPTED MANUSCRIPT
Journal of Applied Physics
AIP Publishing
This is the author's peer reviewed, accepted manuscript. However, the online version of record will be different from this version once it has been copyedited and typeset.
PLEASE CITE THIS ARTICLE AS DOI: 10.1063/5.0151255

The closing rate C is taken to be constant, and the opening rate is taken to be an exponential of the cleft Ca concentration given by λ* exp(γ[Ca]) fitted to experimental data of Laver et al. [13] in our previous study [17]. The analogues of magnetic field *h* and inverse temperature β are given by $\beta = \frac{\gamma\psi(U)}{4}$ and

$$h = \frac{1}{2\beta}\ln\frac{\lambda}{C} + \sum_{\substack{x\neq 0 \\ x\in CRU}} \phi(|x|) \qquad (2)$$

where *U* is the distance between RyRs, ψ is the Ca level in the cleft resulting from the opening of an RyR as a function of distance from the open RyR (i.e. an interaction profile, Fig. 1), and, for any real number *r* (unitless), $\phi(r)= \psi(rU)/(\psi(U))$ is a natural choice of scaling for the interaction profile function ϕ. Upon construction of the isomorphic mapping between the CRU and an Ising model, we see that *h* and β as given above for the CRU play the identical role in the equations as they do in the Ising model. Thus, various properties that are known for the Ising model will carry over to the CRU, in particular the order-disorder phase transition in β and the influence of magnetic field *h*. This has been studied in depth in [35].

3. Results

3.1. The new Markov chain.

We follow an evolution of a cluster under the conditions of strong interactions (i.e. supercritical β) and favorable magnetic field (i.e. positive and growing) but an initial configuration where all RyRs are closed (maximally unfavorable). For a wide range of positive magnetic field *h*, this initial condition constitutes a local energy minimum (also known as a metastable state) and the system is highly unlikely to transition to an all-open state. It would require the unlikely event of several RyRs randomly opening next to each other, despite the closed neighbors. Only when *h* is large enough that one open RyR creates enough Ca flux to strongly influence its neighbors, a spark has a good chance of activating.

To quantify these concepts, we introduce a new Markov chain. We define an *open cluster* as a collection of channels that are open and adjacent (diagonals don't count). The states of the Markov chain are the size of the open cluster going from 0 to 4 (Fig. 2(a)) and the transition probability for increasing the cluster is computed from Equation (1), but weighted by the relative frequency of configurations both in the initial and the target states. The transition probability of decreasing the cluster is computed from Equation (1) as well, but we assume that when transitioning from 3 to 2 only the outside RyRs can close, resulting in the configuration as in state 2. This assumption is reasonable because the gating of the release channels, including its closing rates ofvary strongly under different conditions [2, 13, 43].

3.2. Calculation of transition probabilities.

The Markov model we use is the lumped Markov model, see for example Theorem 6.4.1 in Section 6.4 of [44]. Lumpability means that it is possible to define the probability of

ACCEPTED MANUSCRIPT

Journal of Applied Physics

AIP Publishing

This is the author's peer reviewed, accepted manuscript. However, the online version of record will be different from this version once it has been copyedited and typeset.

PLEASE CITE THIS ARTICLE AS DOI: 10.1063/5.0151255

going from one "lump" of states to another independently of how you got to the starting lump. That ensures that the transition probability between lumps depends only on the lumped state, i.e. which lump you start from, so that the lumped process is a Markov process. This construction would be directly applicable to our setup, if the probability of transitioning from configuration A to a 4-channel configuration (denoted P(A-> 4)) were equal to the probability of transitioning from configuration B to a 4-channel configuration (denoted P(B->4)). Since these probabilities are not equal, we have performed the computation of spark probability for two cases: Case 1 setting both probabilities equal to P(A-> 4) and Case 2 setting both probabilities equal to P(B->4). The resulting spark probabilities are extremely close as depicted in Fig. S1 in supplementary material. We expect the true probability to lie between them. Lastly, we notice that the transition probabilities back from state 3 to 2 are the same for the two configurations in state 3 which satisfies the condition of strong lumpability.

Here we show an example of a calculation for the transition matrix of the lumped Markov process. We compute the probability of going from 1 open channel to 2 open channels $P(1 \rightarrow 2)$ at an SR level of 300 µM. We find the following:

β at 300 µM: 0.6454
$\Sigma_{y \epsilon \Delta_b} \phi(|x-y|)\sigma(y)$ at 300 µM: -20.79
h at 300 µM: 18.02
C (closing channel rate) = 117 s^{-1}
$\Delta t = 7 * 10^{-10}$ ms

$$P(1 \rightarrow 2) = \Delta t C e^{2\beta(\Sigma_{y\epsilon\Delta_b} \phi(|x-y|)\sigma(y)+h)} = (7 * 10^{-10})(117)e^{2(0.645)(-20.79+18.02)}$$
$$= 2.297 * 10^{-9}$$

Lastly, since there are four different ways for one open channel to turn into two open (adjacent) channels, we multiply this probability by four to arrive at the final answer of

$$P(1 \rightarrow 2) = 9.188 * 10^{-9}$$

The calculation becomes more involved for $P(2 \rightarrow 3)$. We have a formula for transition probability from a given configuration to a configuration with one square added. Looking at Fig. 2(b), to compute $P(2 \rightarrow 3)$, we compute the probability of transitioning from a configuration with 2 squares to configuration A (in the left branch) and multiply it by 4 and then add the probability of transitioning from a 2 to configuration B (in the right branch) and multiply by 2. Lastly, there are two ways obtain $P(3 \rightarrow 4)$: one is a weighted sum of probabilities of transitioning from configuration A to a configuration of 4 squares and the second is the appropriately weighted sum of probabilities of transitioning from configuration B to a configuration of 4 squares. This procedure results in a two possible transition matrices $M = (P(i \rightarrow j))_{0 \le i, j \le 4}$, as mentioned above (see also Fig. S1 in supplementary material).

If we take $^{45}{}_{0 \le j \le 4}$ to be the standard basis vectors numbered from 0 to 4 according the states, i.e. having 1 in position corresponding to the given state j and 0's everywhere else, the probability of getting absorbed in state 4 when starting from state 0. Then the probability of ending up in a particular state after starting in state j is given by the vector $\mathbf{e}_j M^k$. To compute the probability of getting absorbed in state 4, we diagonalize the transition matrix M, i.e. we find an orthogonal matrix U and a diagonal matrix D such that $M = UDU^t$. Since there are two states that are absorbing, two eigenvalues will be 1 and others will be smaller than 1. We order the eigenvalues and the corresponding eigenvectors so that the two eigenvalues that are

ACCEPTED MANUSCRIPT
Journal of Applied Physics
AIP Publishing
This is the author's peer reviewed, accepted manuscript. However, the online version of record will be different from this version once it has been copyedited and typeset.
PLEASE CITE THIS ARTICLE AS DOI: 10.1063/5.0151255

1 are last. Then as $k \rightarrow \infty$, D^k will tend to a matrix with two 1's at the bottom of the diagonal and zeros otherwise. We will call this matrix D^∞. The probability of getting absorbed in state 4 after starting in state 1 therefore will be the fourth entry in the vector $\mathbf{e}_1 U D^\infty U^t$ (for implementation see our Python code in supplementary material).

3.3. Model predictions

Figure 3(a) shows the results of our analytical model. For various values of SR Ca we have plotted the conditional probability of transitioning from 2 open channels to 3 open channels conditioned on not staying in state 2 (solid curve) and the similar conditional probability of transitioning from 3 open channels to 4 open channels. Since there are two possible configurations with 3 open channels, we plot both of these in Fig. 3(a): the dotted line shows the probability from triangle-like configuration A in Fig. 2(b) and the dashed line shows the probability from straight configuration B. We notice that both curves $P(3 \rightarrow 4)$ are steeper and lie to the left of $P(2 \rightarrow 3)$, so SR Ca at which the transition from 2 open channels to 3 open channels becomes somewhat likely is the same as SR Ca where the transition from 3 open channels to 4 open channels becomes extremely likely. This indicates the dependence of growth of the open cluster on its size. On a physics level, this happens because the system with all channels closed but positive magnetic field and supercritical β is in a local energy minimum. Each individual channel or small cluster might not open or, if open, close quickly due to the strong interaction from closed neighbors. But as the open cluster grows, the "curvature" of its boundary decreases, so the effect from the closed neighbors gets distributed over more open neighbors and is less likely to close an open channel.

The probability of the initial recruitment follows a steep sigmoid curve as a function of SR Ca load, beginning to rise at around 250 μM. Our analytic results (Fig. 3(b), circles) match the results of our numerical simulations (Fig. 3(b), triangles) and experimental studies (Fig. 3(c)). More sensitive spark generation at high SR Ca vs. numerical estimates reflects analytical model assumption of instantaneous interactions, whereas Ca diffusion causes a small delay. In numerical model it takes roughly 2.5 ms for the Ca profile to reach its stable level (Figure 2B of [17]). Approximating the interactions with a step-function which is 0 until 1.25 ms and the full profile after 1.25 ms, and using the closing rate from our numerical model of $C=0.117\ \mathrm{ms}^{-1}$, we obtain that with probability of approximately 15% the RyR will close before it has a chance to interact with other channels. On the other hand, with probability of 85% it will interact and enter into our Markov chain setup. Thus, we scaled the curve by 0.85 to account for this discrepancy and obtained a closer match at higher SR Ca (Fig. 3(b), diamonds). Less sensitive spark generation at low SR Ca in analytical model can be due to other Ising model assumptions, such as its interactions limited to the nearest neighbors. On the other hand, the threshold of spark activation (300-400 μM) reported in experimental studies (Fig. 3(c)) is better reproduced by our analytical model than by the numerical modeling (200-300 μM).

While our model was examined for only one specific set of parameters fitted to experimental data of Laver et al. [13], we want to know how the SR Ca threshold for spark initiation will depend in general on the variety of possible variations of model parameters determining the RyR opening rate that can be present in variety of experimental, physiological and pathological conditions in different species. Figure 4 shows the results of a 2-dimensional sensitivity analysis of the SR Ca threshold for spark initiation with respect to parameters λ and γ in both analytical (a) and numerical (b) models; the opening rate (k) is taken to be an exponential of the cleft [Ca] given by $k = \lambda * \exp(\gamma[\mathrm{Ca}])$. The two models

ACCEPTED MANUSCRIPT
Journal of Applied Physics
AIP Publishing
This is the author's peer reviewed, accepted manuscript. However, the online version of record will be different from this version once it has been copyedited and typeset.
PLEASE CITE THIS ARTICLE AS DOI: 10.1063/5.0151255

predicted the phase transition for spark activation as the function of SR Ca in a wide range of parametric space, but no phase transition with respect to λ and γ (graduate color changes in Fig. 4).

Thus far, we performed our simulations with fixed SR Ca levels and initial RyR opening in the center of the grid. In reality, RyR can open at any location and when the system progresses to spark activation (assumed at 4 open channels), the SR Ca level gets slightly depleted (by ~3.5% in the example of numerical simulations in Fig. 5 and Videos S1 and S2 in supplementary material). Thus, a more realistic probability curve for the threshold SR Ca level that takes into account these factors is expected to be shifted to larger values. Furthermore, previous studies also showed that spark behavior depends substantially on RyR cluster size [34, 46, 47]. Therefore, we performed additional numerical simulations comparing the emergence of sparks with free running SR vs. fixed SR for various sizes of clusters of interacting RyRs with initial opening of RyR in a random location (Fig. 6). Our first finding was that the SR spark activation threshold increases as the size decreases. Furthermore, the difference between simulations with free-running vs. fixed SR was most pronounced for small cluster sizes and less so for larger ones. We found that for an 11x11 cluster, the shift of the spark activation threshold was rather small from about 220 μM to 250 μM. Our respective simulations using our standard CRU model of 9x9 RyR cluster showed a notable shift of the threshold from 250 μM to about 300 μM (black dashed curve vs. solid curve in Fig. 6A). The shift increased for 7x7 cluster (from 300 μM to 400 μM), and further substantially increased (from 400 μM to 650 μM) for the smallest cluster of 5x5 we tested. We summarized our results with various sizes of RyR clusters in Fig. 6B and fitted them with a power function.

4. Discussion

The present study provides a mechanistic view on the spark initiation threshold in a CRU system of interacting RyRs via local CICR. Mathematically speaking, one can view spark activation as equivalent to a system transitioning from a local energy minimum (also known as a metastable state) to a global one. Thus, spark activation is analogous to the pressure required to overcome surface tension in bubble formation. When an open cluster forms in a background of closed channels, the interaction between the closed and the open channels happens only at the boundary of the open cluster. When the open cluster is small, there are more closed channels per open channel at the boundary. As the open cluster gets bigger, this ratio gets more favorable for the open channels. This reflects the “curvature” of the boundary as in bubble formation. This interpretation is reasonable for a large variety of model parameter values, as the SR Ca threshold varies continuously with the model parameters (Fig. 4).

In this study, we use numerical and analytical approaches to study Ca spark activation. We examined spark activation at different fixed SR Ca levels and found a sharp transition at about 300 μM level where sparks were robustly generated. Zima et al. [30] reported spark and non-spark Ca SR leak types in ventricular myocytes. As SR Ca load grows above ~300 μM, Ca sparks contribute to the leak in a liner fashion (Fig. 3(c)). We further performed simulations for more realistic scenarios with free-running SR in which Ca gets depleted as RyRs open and also for a wide variety of different RyR cluster sizes (Figs 5 and 6). The spark activation threshold is shifted towards larger values as cluster size decreases mainly due to boundary effects: 1) the interaction profile of an open RyR decreases for smaller CRU sizes in general and especially for the RyRs in the CRU periphery, as released Ca quickly leaks to

Journal of Applied Physics
AIP Publishing
ACCEPTED MANUSCRIPT
This is the author's peer reviewed, accepted manuscript. However, the online version of record will be different from this version once it has been copyedited and typeset.
PLEASE CITE THIS ARTICLE AS DOI: 10.1063/5.0151255

cytoplasm via the CRU boundary; 2) the relative contribution of RyRs at the CRU boundary increases as CRU size decreases. Thus, in a real cell, for a given SR Ca level, the activated sparks will be coming from all the clusters with sizes whose thresholds are below the given level. For example, at 300 μM sparks from CRUs of sizes more than 81 will be contributing to the total spark mediated leak, at 400 μM the CRUs of sizes more than 49 will contribute, and finally near 650 the 25's will start contributing to the total. Considering also that cluster sizes are heterogeneous [48], we expect that this will yield the near linear growth of spark-mediated leak flux evident in experimental data (Fig. 3(c)).

Our model includes measurable parameters of the system that can be further varied to understand the impact of realistic factors for spark activation. These are present in our model via their impact on the Ca profiles, numerically generated by Stern model [16]. Such factors include SERCA pumping rate to increase SR Ca, connectivity of free SR and junctional SR [49], Ca buffering (e.g. via calsequestrin), phosphorylation of key Ca cycling molecules, etc. While spontaneous Ca release during diastole can trigger life-threating arrythmia [23], the increased diastolic Ca release contributes to normal generation of spontaneous pacemaker potentials driving the heartbeat [3]. Thus, our approach could help in directing pharmacological interventions to avoid regimes of spontaneous spark activation in cardiac muscle cells in cardiac disease [23] or to promote such regimes in cardiac pacemaker cells in sick sinus syndrome (insufficient pacemaker function) [50]. Lastly, our new analytical approach provides a substantial computational advantage to evaluate the conditions for spark activation within Ca release channel clusters. Calculating the dynamics for all states in the full Markovian representation of a CRU using the analytic solution to Markov matrix would involve taking exponentials of enormously large matrices. Thus, the benefits of this novel approach are to get insight into RyR system behavior using minimal computational cost.

5. Study limitations

We assume that once the open cluster reaches 4 in size, it always initiates a spark and we call the size 4 cluster the initial recruitment. We do not compute the probability of transitioning from 4 to 5, we call it $P(4 \rightarrow 5)$, because the enumeration of all the possible clusters becomes cumbersome. However, it is clear that the curve $P(4 \rightarrow 5)$ as well as further curves such as $P(5 \rightarrow 6)$ would be much steeper and lie to the left of $P(3 \rightarrow 4)$, in a similar way as $P(3 \rightarrow 4)$ is steeper and lies to the left of $P(2 \rightarrow 3)$ as evidenced in Fig. 3(a). Thus, it is reasonable to let 0 and 4 be absorbent states. We also assume that from a state of 3 open channels only two of the channels (the ones closest to the outside) can close. This will have skewed our results slightly toward activation, but the effect will be small and within the range of uncertainty caused by variability in RyR closing rates.

Supplementary Material

1. Supplementary text: Mathematical formulations mapping a CRU to Ising model

2. Supplementary figure S1

3. Supplementary computer code: Python code that computes the probability that a spark initiates from a given open RyR at various SR Ca

ACCEPTED MANUSCRIPT
Journal of Applied Physics
AIP Publishing
This is the author's peer reviewed, accepted manuscript. However, the online version of record will be different from this version once it has been copyedited and typeset.
PLEASE CITE THIS ARTICLE AS DOI: 10.1063/5.0151255

4. Supplementary data: the table of interaction profiles at various SR Ca (ψ values) needed to run the Python code

5. Supplementary videos:

Video S1

Top panel: an example of Ca spark generated by our numerical model, including activation and termination. The spark is generated by a 9x9 square grid of RyR channels. Initial SR Ca = 1 mM. [Ca] is coded by red shades: 0 is pure black, 30 μM is pure red. The spark evolves from one open channel. Closed channels are shown by green arrows and open channels are shown by white arrows. Low panel: simultaneous time course of number of open RyRs.

Video S2

The same spark as in Video 1 but shown at a finer time scale to clearly display activation phase and evolution of open RyR configurations (described in Fig. 2). [Ca] is coded by red shades: 0 is pure black, 200 μM is pure red. Time and # of open RyRs are shown in the top.

Acknowledgements

The work was supported by the Intramural Research Program of the National Institute on Aging, National Institutes of Health. A.V.M. acknowledges support of the Royal Society University Research Fellowship UF160569.

AIP Publishing
Journal of Applied Physics
ACCEPTED MANUSCRIPT
This is the author's peer reviewed, accepted manuscript. However, the online version of record will be different from this version once it has been copyedited and typeset.
PLEASE CITE THIS ARTICLE AS DOI: 10.1063/5.0151255

Figures and figure legends

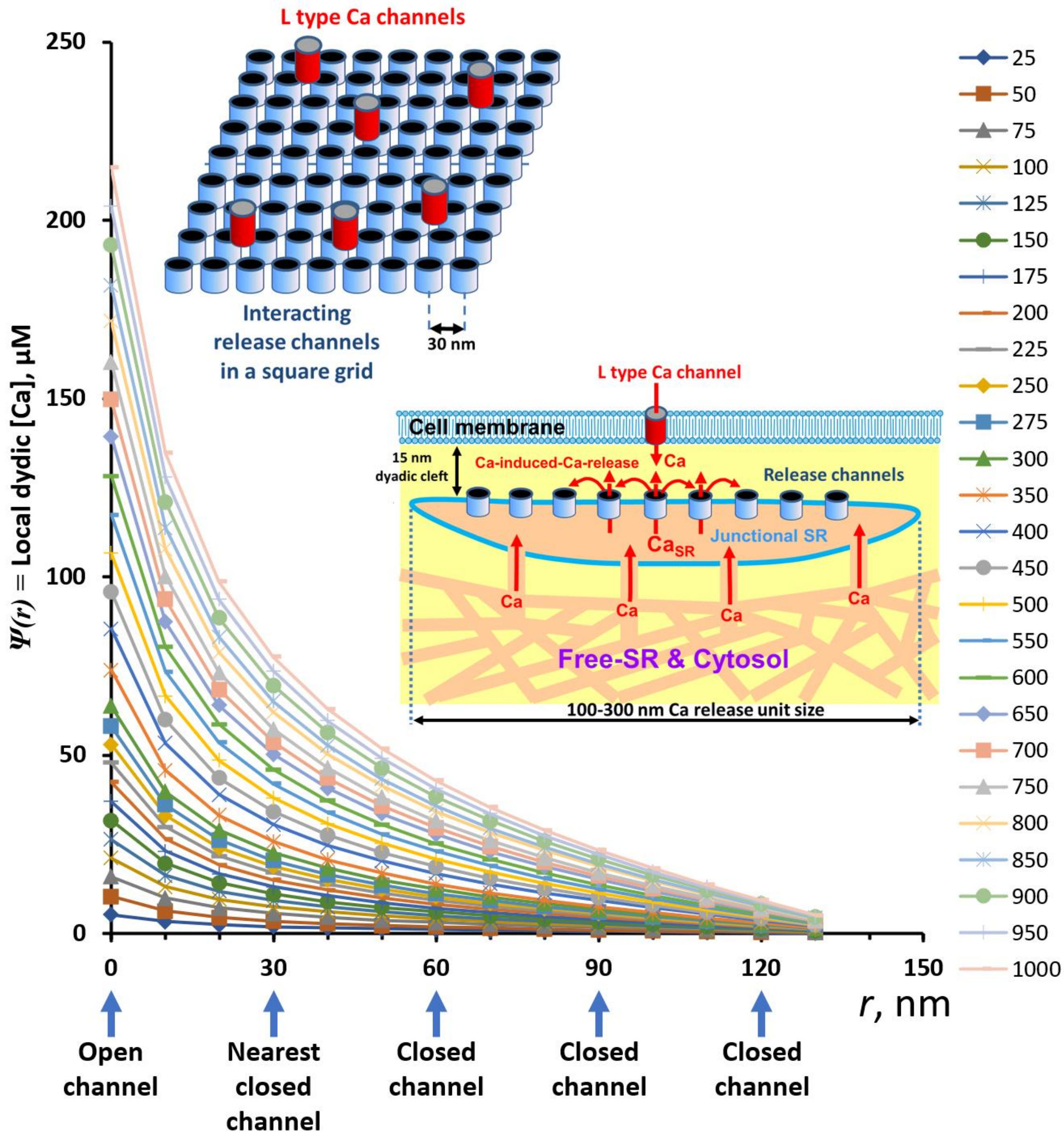

Figure 1. The definition and numerical simulations of RyR interaction profile *ψ(r)* that determines Ca-induced-Ca release in our model. . *ψ(r)* is a steady-state [Ca] in the dyadic cleft as a function of distance *r* when one RyR opens at *r*=0. The plot shows is a family of simulated interaction profiles *ψ(r)* at various fixed SR Ca loadings from 25 to 1000 μM (right column shows lines and symbols for each curve). Larger [Ca] at the nearest closed channel at higher SR loading indicates stronger channel interactions and stronger Ca-induced-Ca release. The interaction profiles were measured in numerical simulations of sparks as an instantaneous [Ca] in dyadic space 10 ms after the first channel opens for 9x9 RyR grid, the distance between RyRs is 30 nm, and each voxel is 10x10x15 nm in xyz. All other channels were forced to stay closed. See supplemental Excel file for exact values of the profiles that were used in our simulations of analytical model. Insets (modified from [17]) show the RyR grid and its location with respect to SR, cytoplasm, and cell membrane in our CRU model. Please note that L-type channels are not included in our model of spark activation.

ACCEPTED MANUSCRIPT
Journal of Applied Physics
AIP Publishing
This is the author's peer reviewed, accepted manuscript. However, the online version of record will be different from this version once it has been copyedited and typeset.
PLEASE CITE THIS ARTICLE AS DOI: 10.1063/5.0151255

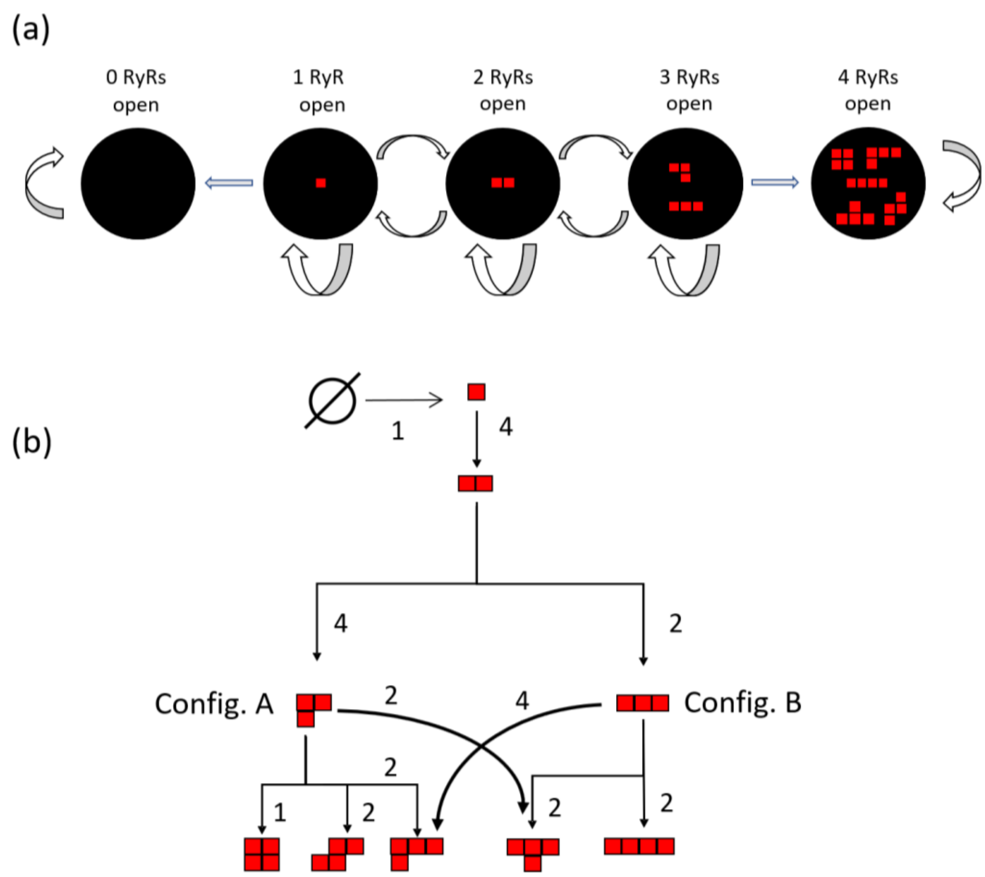

Figure 2. Our model includes all possible spatial configurations of RyR openings during initial interaction steps of spark activation after one channel is open acting as a nucleation site. (a) Schematical illustration of five-state Markov process simulating the spark evolution in our weakly lumped model. Each arrow represents the event of the Markov process changing from one state to another state with the direction indicated by the arrow. Each black circle shows all possible configurations of open RyRs, independent of how each configuration was reached. **(b)** Configuration tree. Illustration of all possible configurations and the series of events that could take place to reach each of the configurations. The model has 10 possible configurations, including configuration Ø with no open channels. Numbers at each configuration indicate the number of possible ways to reach a given configuration.

ACCEPTED MANUSCRIPT
Journal of Applied Physics
AIP Publishing
This is the author's peer reviewed, accepted manuscript. However, the online version of record will be different from this version once it has been copyedited and typeset.
PLEASE CITE THIS ARTICLE AS DOI: 10.1063/5.0151255

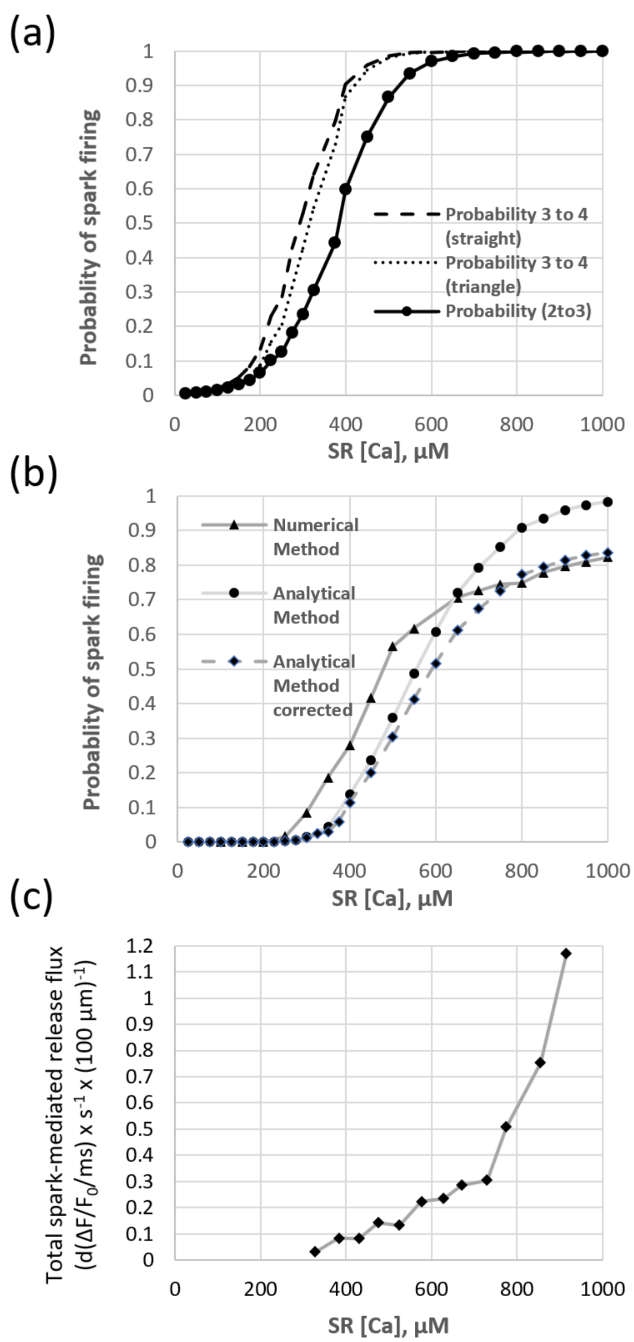

Figure 3. Our analytical and numerical models predict the probability of Ca spark activation as a function of SR Ca loading. (a): The probability of transitioning from 2 open channels to 3 open channels (circles) and probabilities of transitioning from 3 open channels to 4 open channels via straight configuration (dash line) or triangle configuration (dotted line). **(b)**, Spark activation predicted numerically and analytically with and analytically without correction for diffusion delay. In numerical method, probability of spark firing at each SR Ca was evaluated from 10,000 simulation runs of 200 ms each. In each run at t=0 one RyR in the center of 9x9 RyR cluster was set open. Our criterion for spark firing was that 50% of all RyRs open at any moment before all RyRs closed. **(c),** Experimentally defined SR Ca threshold for Ca spark activation; shown are mean values of total spark-mediated release flux (measured by confocal microscopy) which were rescanned and replotted from Figure 3B of [30].

ACCEPTED MANUSCRIPT
Journal of Applied Physics
AIP Publishing
This is the author's peer reviewed, accepted manuscript. However, the online version of record will be different from this version once it has been copyedited and typeset.
PLEASE CITE THIS ARTICLE AS DOI: 10.1063/5.0151255

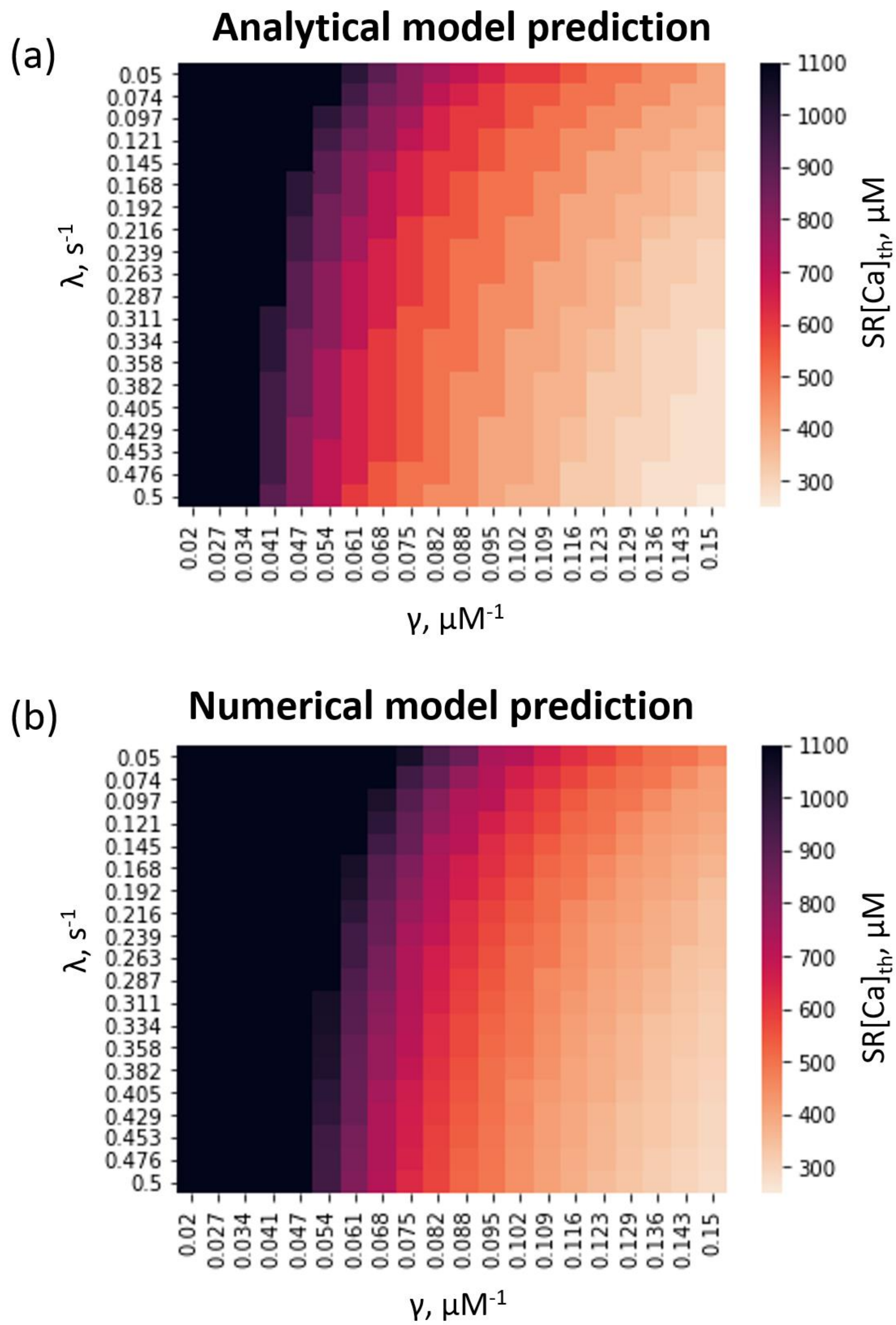

Figure 4. Numerical and analytic models behave essentially the same within a broad range of key model parameters λ and γ. Shown are heatmaps of two-dimensional sensitivity analysis of the SR Ca threshold ($SR[Ca]_{th}$) for spark initiation with respect to λ and γ in analytical (a) and numerical (b) models; the RyR opening rate is taken to be an exponential of the cleft [Ca] given by λ* exp(γ[Ca]). For these analyses we set 0.1 probability for spark activation to obtain the associated SR Ca threshold. In turn, in numerical simulations each threshold was defined from a series of spark activation simulation with increasing SR Ca, and probability of spark firing at each SR Ca was evaluated from 10,000 simulation runs.

ACCEPTED MANUSCRIPT
Journal of Applied Physics
AIP Publishing
This is the author's peer reviewed, accepted manuscript. However, the online version of record will be different from this version once it has been copyedited and typeset.
PLEASE CITE THIS ARTICLE AS DOI: 10.1063/5.0151255

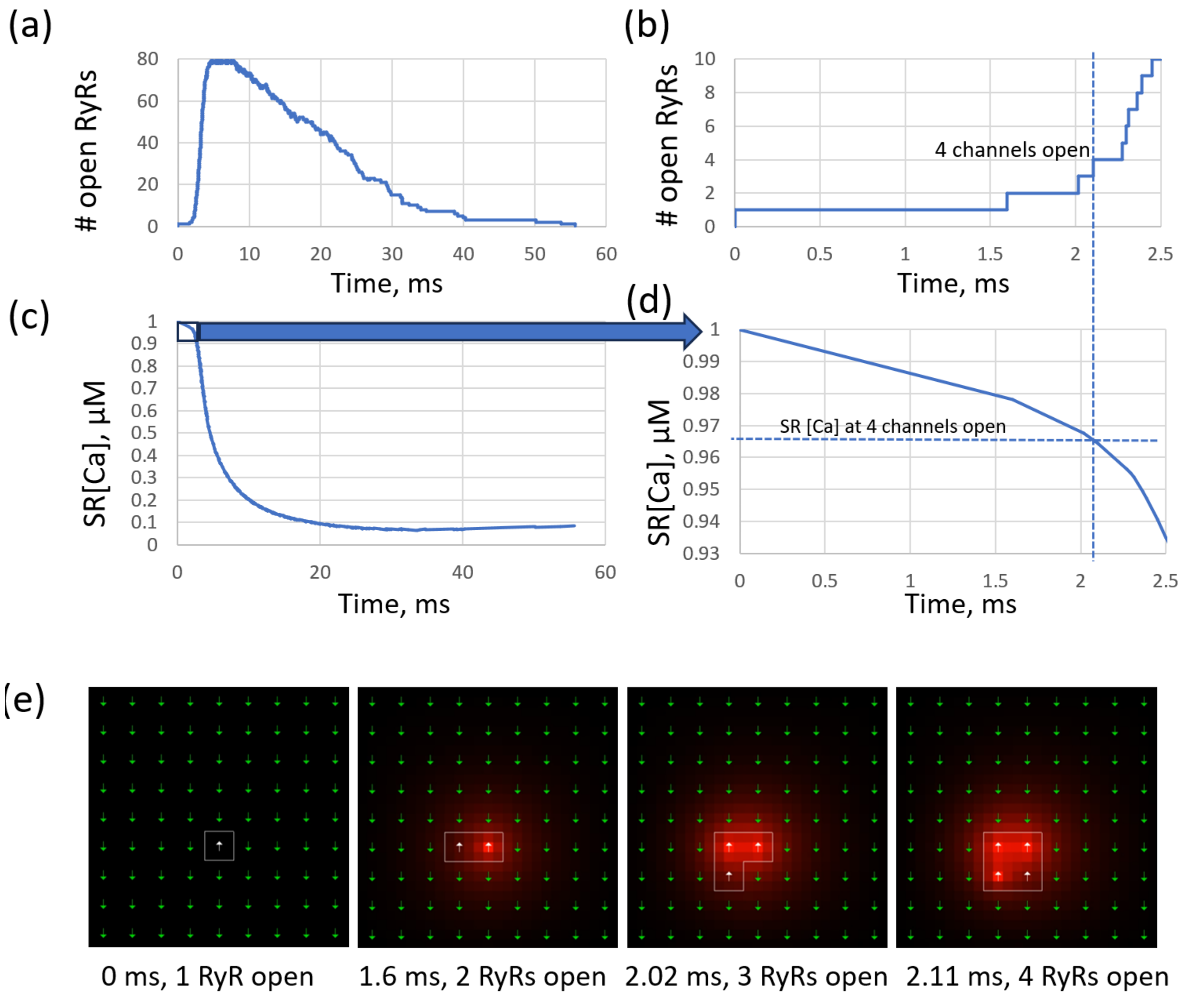

Figure 5. An example of numerical model simulation of a Ca spark evolution triggered by an opening of one RyR at Time=0 at a random location. (a), Number of open RyRs as a function of time for the entire duration of the spark. **(b)** RyR openings for the first 2.5 ms. **(c)**, SR Ca depletion during the entire duration of the spark. **(d)**, A minor SR Ca depletion at the moment when 4 channels open. **(e)**, Detailed spatiotemporal CRU system evolution from one open channel (white arrow) to 4 open channels in 9x9 RyR grid. The open channel cluster is outlined by white line. In this example, the spark activation evolves via 3 transitions, recruiting to fire its neighbors counterclockwise. Channels are shown by green arrows. [Ca] is coded by red shades: 0 µM is pure black and 200 µM is pure red. See more details in Supplementary Videos S1 and S2.

ACCEPTED MANUSCRIPT
Journal of Applied Physics
AIP Publishing
This is the author's peer reviewed, accepted manuscript. However, the online version of record will be different from this version once it has been copyedited and typeset.
PLEASE CITE THIS ARTICLE AS DOI: 10.1063/5.0151255

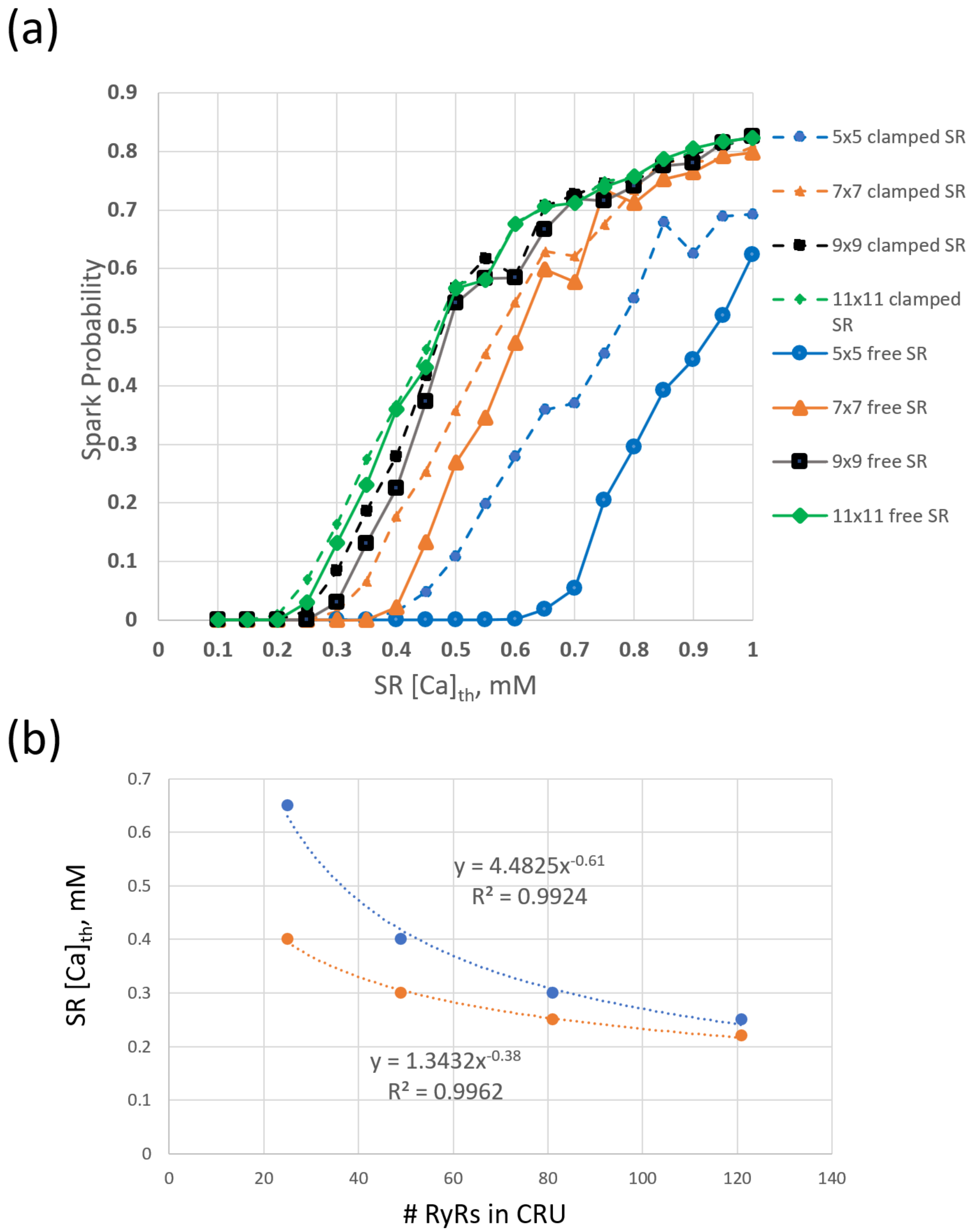

Figure 6. Numerical model prediction of probability of Ca spark activation as a function of SR Ca loading for RyR clusters of various sizes. (a), Spark probabilities with fixed SR Ca (dashed lines) vs. free-running SR, i.e. SR Ca was not fixed (solid lines). For each data point, probability of spark firing a was evaluated from 10,000 simulation runs of 200 ms each. In each run at t=0 one RyR in a random location in respective RyR cluster was set open. **(b),** SR Ca threshold as a function of number of RyRs in CRU fitted with a power function (equations with R^2 values are shown at the plots).

ACCEPTED MANUSCRIPT
Journal of Applied Physics
AIP Publishing
This is the author's peer reviewed, accepted manuscript. However, the online version of record will be different from this version once it has been copyedited and typeset.
PLEASE CITE THIS ARTICLE AS DOI: 10.1063/5.0151255

References

1. A. Fabiato, Am J Physiol **245** (1), C1-14 (1983).
2. H. Cheng and W. J. Lederer, Physiol Rev **88** (4), 1491-1545 (2008).
3. E. G. Lakatta, V. A. Maltsev and T. M. Vinogradova, Circ Res **106**, 659-673. (2010).
4. M. G. Klein and M. F. Schneider, Prog Biophys Mol Biol **92** (3), 308-332 (2006).
5. H. A. T. Pritchard, P. W. Pires, E. Yamasaki, P. Thakore and S. Earley, Proc Natl Acad Sci U S A **115** (41), E9745-E9752 (2018).
6. G. Fan, Y. Cui, M. Gollasch and M. Kassmann, Channels (Austin) **13** (1), 505-519 (2019).
7. J. Zmazek, M. S. Klemen, R. Markovic, J. Dolensek, M. Marhl, A. Stozer and M. Gosak, Front Physiol **12**, 612233 (2021).
8. V. N. Friedhoff, R. Ramlow, B. Lindner and M. Falcke, The European Physical Journal Special Topics **230**, 2911–2928 (2021).
9. Z. Qu, A. Garfinkel, J. N. Weiss and M. Nivala, Prog Biophys Mol Biol **107** (1), 21-31 (2011).
10. M. Gosak, R. Markovic, J. Dolensek, M. Slak Rupnik, M. Marhl, A. Stozer and M. Perc, Phys Life Rev **24**, 118-135 (2018).
11. A. V. Maltsev, V. A. Maltsev, M. Mikheev, L. A. Maltseva, S. G. Sirenko, E. G. Lakatta and M. D. Stern, Biophys J **100**, 271-283 (2011).
12. M. Nivala, C. Y. Ko, M. Nivala, J. N. Weiss and Z. Qu, Biophys J **102** (11), 2433-2442 (2012).
13. D. R. Laver, C. H. Kong, M. S. Imtiaz and M. B. Cannell, J Mol Cell Cardiol **54**, 98-100 (2013).
14. M. A. Walker, V. Gurev, J. J. Rice, J. L. Greenstein and R. L. Winslow, PLoS Comput Biol **13** (11), e1005783 (2017).
15. Z. Song, A. Karma, J. N. Weiss and Z. Qu, PLoS Comput Biol **12** (1), e1004671 (2016).
16. M. D. Stern, E. Rios and V. A. Maltsev, J Gen Physiol **142** (3), 257-274 (2013).
17. A. V. Maltsev, V. A. Maltsev and M. D. Stern, Proc Natl Acad Sci U S A **114** (29), 7525–7530 (2017).
18. G. S. Williams, A. C. Chikando, H. T. Tuan, E. A. Sobie, W. J. Lederer and M. S. Jafri, Biophys J **101** (6), 1287-1296 (2011).
19. G. Ullah, I. Parker, D. O. Mak and J. E. Pearson, Cell Calcium **52** (2), 152-160 (2012).
20. M. N. I. Patoary, C. Tropper, R. A. McDougal, Z. Lin and W. W. Lytton, IEEE/ACM Trans Comput Biol Bioinform **16** (3), 1007-1019 (2019).
21. M. Gosak, M. Milojevic, M. Duh, K. Skok and M. Perc, Phys Life Rev **41**, 1-21 (2022).
22. P. Petrovic, I. Valent, E. Cocherova, J. Pavelkova and A. Zahradnikova, J Gen Physiol **145** (6), 489-511 (2015).
23. D. M. Bers, Annu Rev Physiol **70**, 23-49 (2008).
24. M. D. Stern, L. A. Maltseva, M. Juhaszova, S. J. Sollott, E. G. Lakatta and V. A. Maltsev, J Gen Physiol **143** (5), 577-604 (2014).
25. C. F. Norris and A. V. Maltsev, Journal of Physics: Complexity **4** (1), 015003 (2023).
26. I. J. Stamper and X. Wang, J Theor Biol **475**, 1-24 (2019).
27. M. Šterk, J. Dolensek, L. Križancic, R. Markovic, J. Zmazek, M. Perc, V. Pohorec, A. Stozer and M. Gosak, Commun Nonlinear Sci Numer Simulat **93**, 105495 (2021).
28. M. S. Islam, Adv Exp Med Biol **1131**, 1-6 (2020).
29. D. X. Brochet, W. Xie, D. Yang, H. Cheng and W. J. Lederer, Circ Res **108** (2), 210-218 (2011).
30. A. V. Zima, E. Bovo, D. M. Bers and L. A. Blatter, J Physiol **588** (Pt 23), 4743-4757 (2010).
31. M. A. Walker, G. S. Williams, T. Kohl, S. E. Lehnart, M. S. Jafri, J. L. Greenstein, W. J. Lederer and R. L. Winslow, Biophys J **107** (12), 3018-3029 (2014).

AIP Publishing Journal of Applied Physics ACCEPTED MANUSCRIPT
This is the author's peer reviewed, accepted manuscript. However, the online version of record will be different from this version once it has been copyedited and typeset.
PLEASE CITE THIS ARTICLE AS DOI: 10.1063/5.0151255

32. E. A. Sobie, K. W. Dilly, J. dos Santos Cruz, W. J. Lederer and M. S. Jafri, Biophys J **83** (1), 59-78 (2002).
33. D. Sato and D. M. Bers, Biophys J **101** (10), 2370-2379 (2011).
34. Y. Xie, Y. Yang, S. Galice, D. M. Bers and D. Sato, Biophys J **116** (3), 530-539 (2019).
35. A. V. Maltsev, M. D. Stern and V. A. Maltsev, Biophys J **116** (11), 2212-2223 (2019).
36. G. Meissner, J Gen Physiol **149** (12), 1065-1089 (2017).
37. A. P. Hill, O. Kingston and R. Sitsapesan, Mol Pharmacol **65** (5), 1258-1268 (2004).
38. I. Zahradnik, S. Gyorke and A. Zahradnikova, J Gen Physiol **126** (5), 515-527 (2005).
39. M. Fill, A. Zahradnikova, C. A. Villalba-Galea, I. Zahradnik, A. L. Escobar and S. Gyorke, J Gen Physiol **116** (6), 873-882 (2000).
40. R. Sitsapesan and A. J. Williams, J Membr Biol **159** (3), 179-185 (1997).
41. A. J. Williams, D. J. West and R. Sitsapesan, Q Rev Biophys **34** (1), 61-104 (2001).
42. R. J. Baxter, *Exactly Solved Models in Statistical Mechanics*. (Academic Press, 1989).
43. D. R. Laver, Biophys J **92** (10), 3541-3555 (2007).
44. J. G. Kemeny and J. L. Snell, Springer New York, NY (1976).
45. Z. Zhang, Y. Xu, H. Song, J. Rodriguez, D. Tuteja, Y. Namkung, H. S. Shin and N. Chiamvimonvat, Circ Res **90** (9), 981-987 (2002).
46. C. Soeller, Proc Natl Acad Sci U S A **115** (41), 10195-10197 (2018).
47. M. Fill and D. Gillespie, Pflugers Arch **473** (3), 435-446 (2021).
48. D. Baddeley, I. D. Jayasinghe, L. Lam, S. Rossberger, M. B. Cannell and C. Soeller, Proc Natl Acad Sci U S A **106** (52), 22275-22280 (2009).
49. D. Sato, T. R. Shannon and D. M. Bers, Biophys J **110** (2), 382-390 (2016).
50. H. Dobrzynski, M. R. Boyett and R. H. Anderson, Circulation **115** (14), 1921-1932 (2007).

ACCEPTED MANUSCRIPT
Journal of Applied Physics
AIP Publishing
This is the author's peer reviewed, accepted manuscript. However, the online version of record will be different from this version once it has been copyedited and typeset.
PLEASE CITE THIS ARTICLE AS DOI: 10.1063/5.0151255

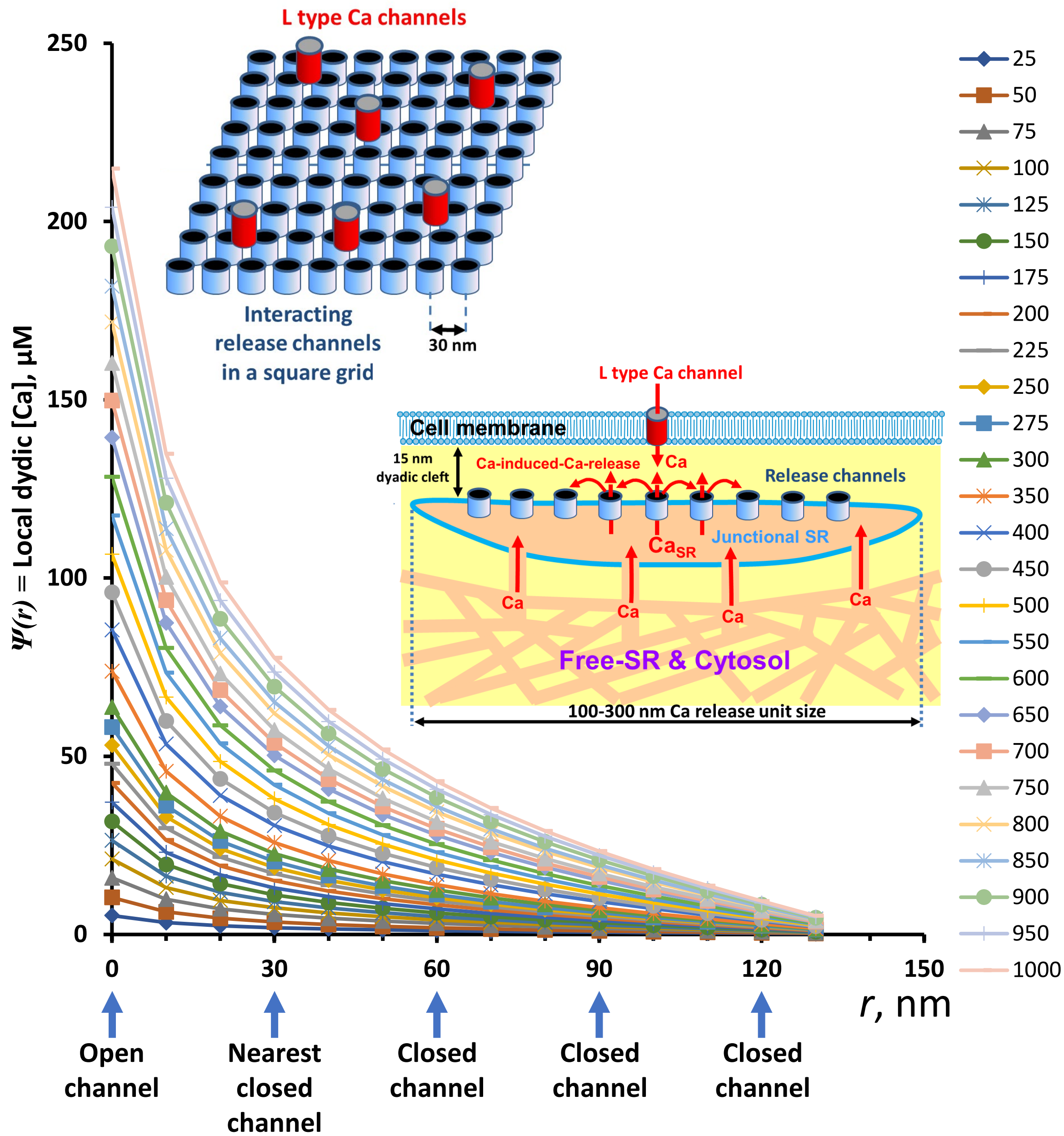

Fig. 1

ACCEPTED MANUSCRIPT
Journal of Applied Physics
AIP Publishing
This is the author's peer reviewed, accepted manuscript. However, the online version of record will be different from this version once it has been copyedited and typeset.
PLEASE CITE THIS ARTICLE AS DOI: 10.1063/5.0151255

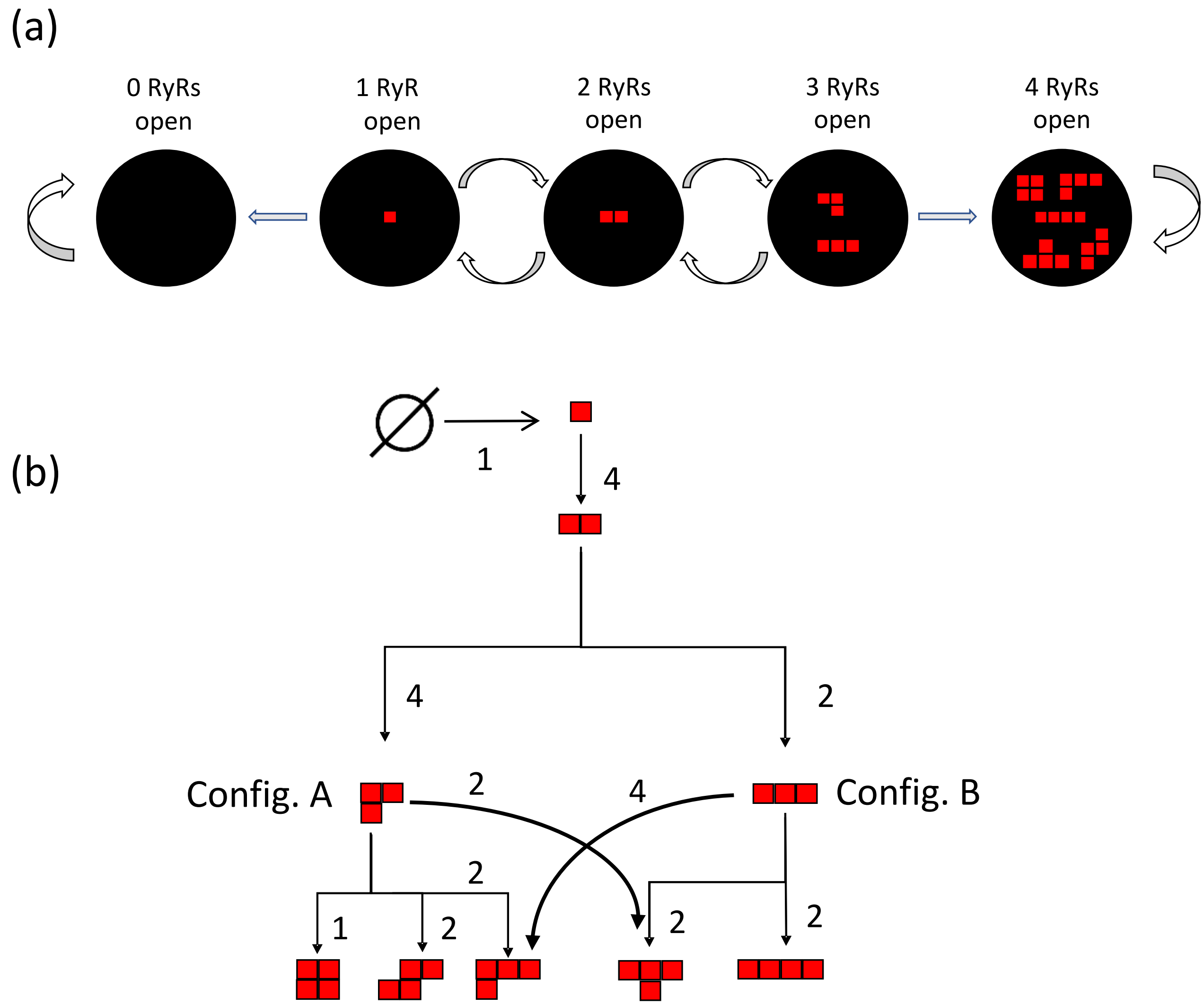

Fig. 2

ACCEPTED MANUSCRIPT
Journal of Applied Physics
AIP Publishing
This is the author's peer reviewed, accepted manuscript. However, the online version of record will be different from this version once it has been copyedited and typeset.
PLEASE CITE THIS ARTICLE AS DOI: 10.1063/5.0151255

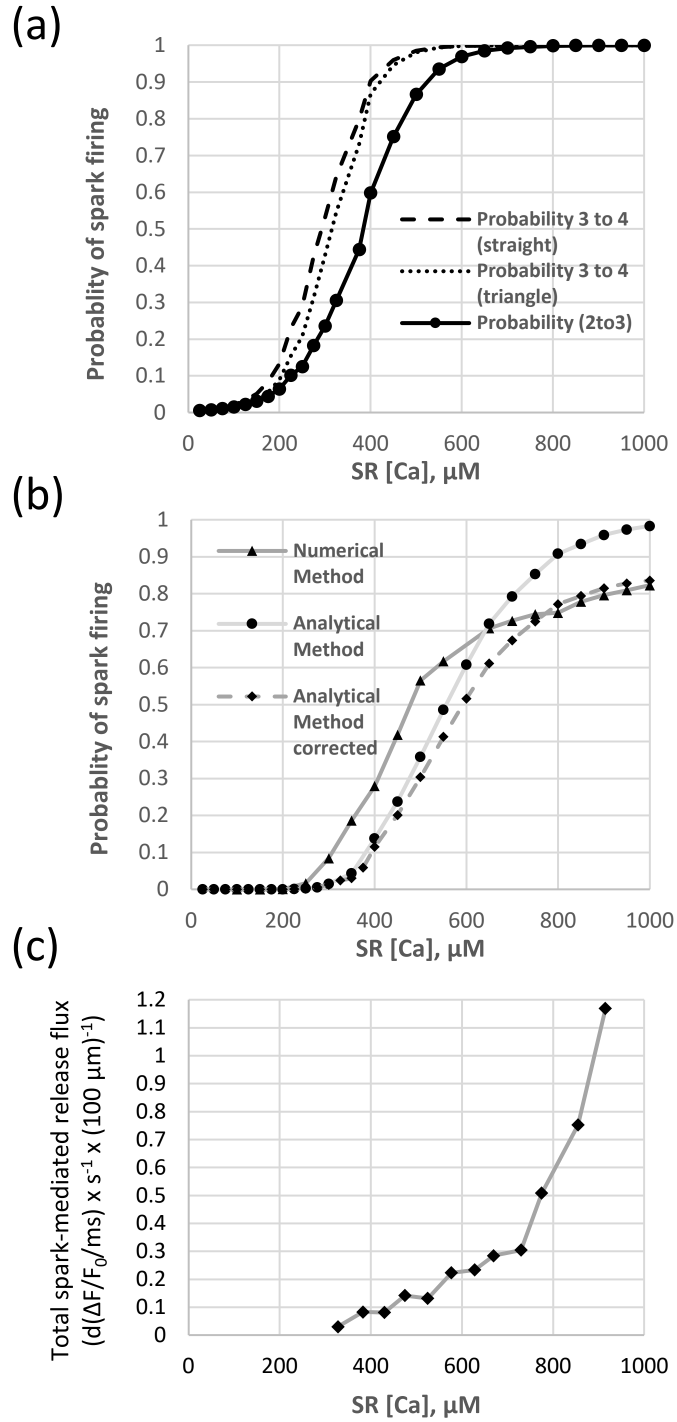

Fig. 3

ACCEPTED MANUSCRIPT
Journal of Applied Physics
AIP Publishing
This is the author's peer reviewed, accepted manuscript. However, the online version of record will be different from this version once it has been copyedited and typeset.
PLEASE CITE THIS ARTICLE AS DOI: 10.1063/5.0151255

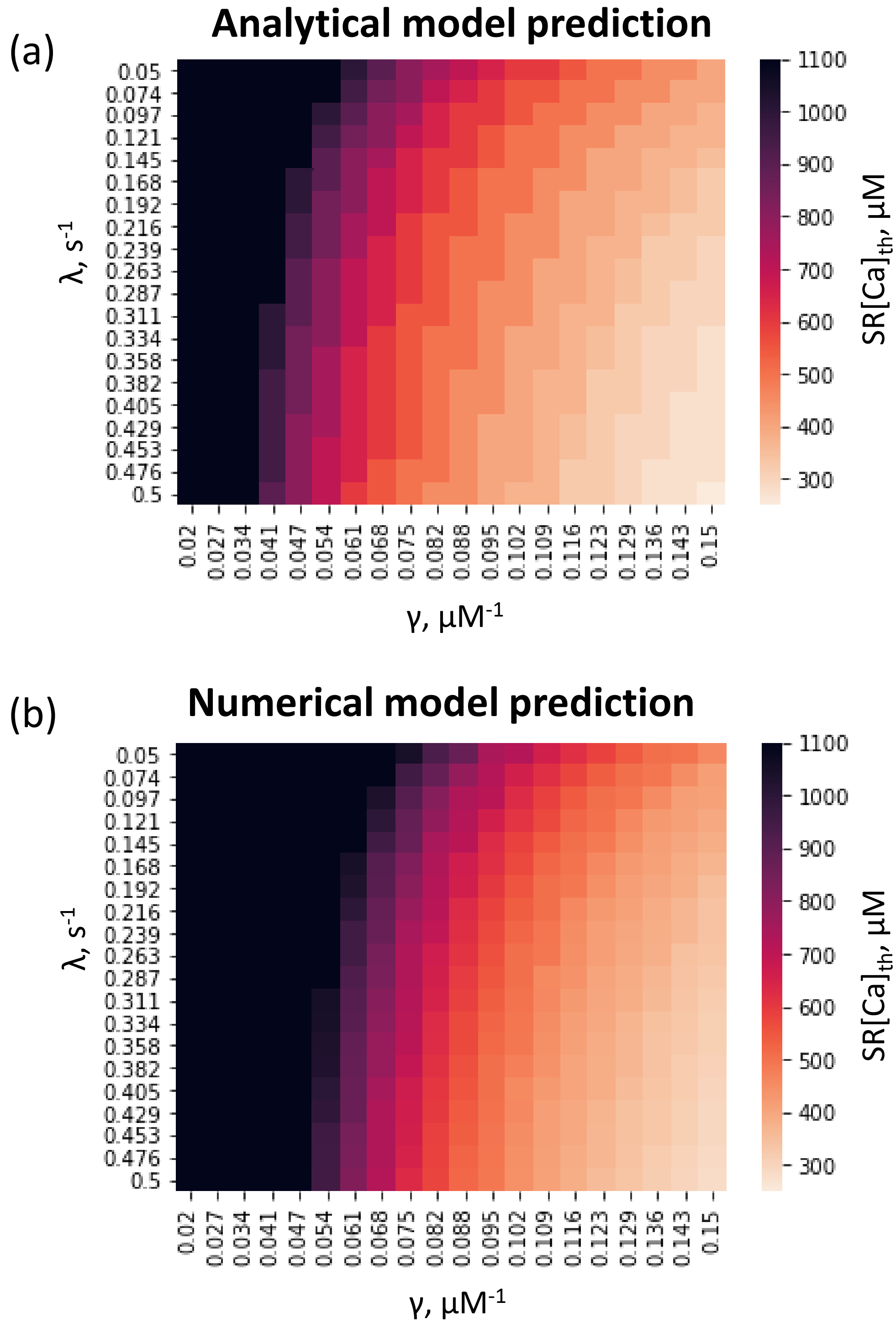

Figure 4

ACCEPTED MANUSCRIPT
Journal of Applied Physics
AIP Publishing
This is the author's peer reviewed, accepted manuscript. However, the online version of record will be different from this version once it has been copyedited and typeset.
PLEASE CITE THIS ARTICLE AS DOI: 10.1063/5.0151255

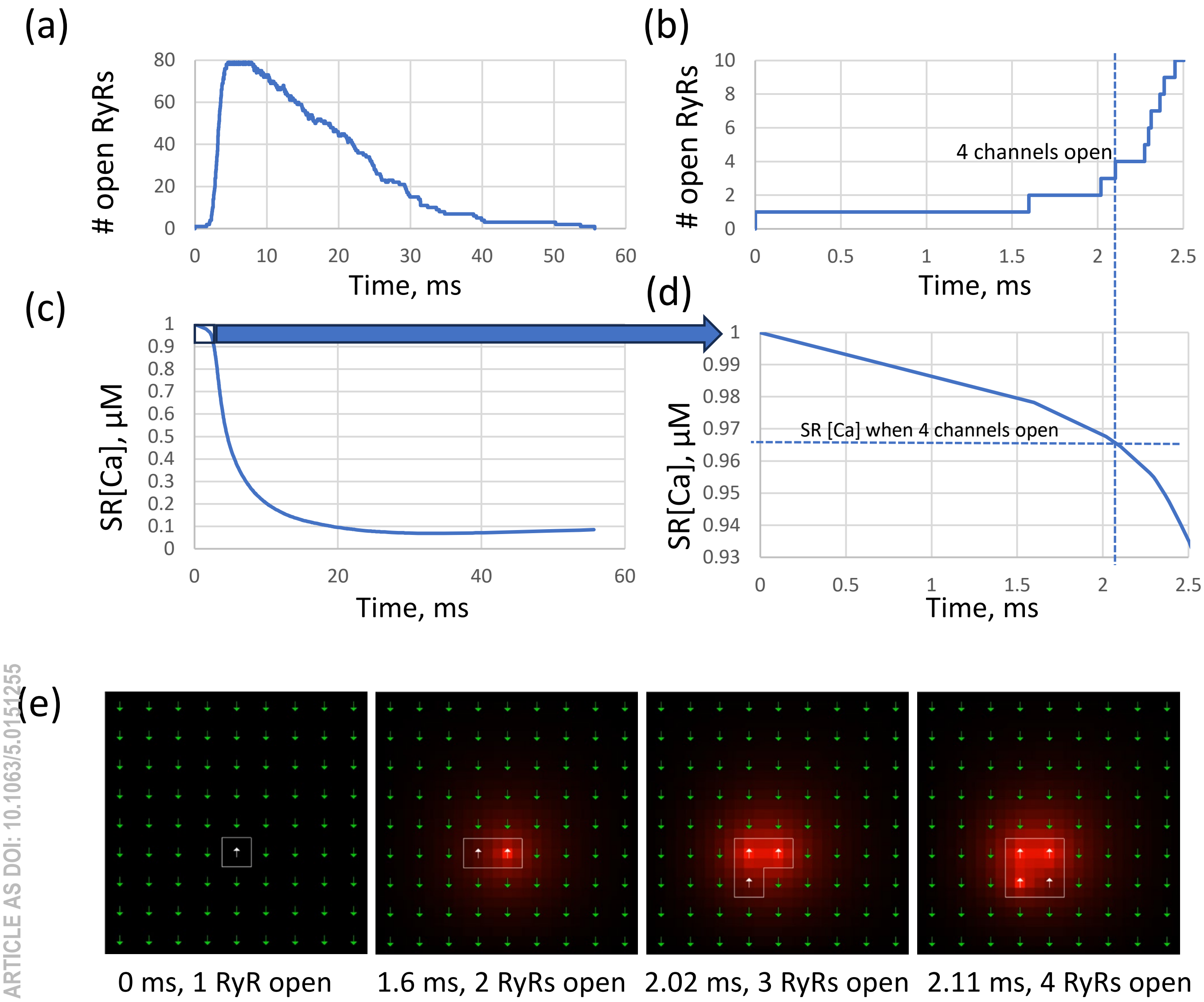

Figure 5

ACCEPTED MANUSCRIPT
Journal of Applied Physics
AIP Publishing
This is the author's peer reviewed, accepted manuscript. However, the online version of record will be different from this version once it has been copyedited and typeset.
PLEASE CITE THIS ARTICLE AS DOI: 10.1063/5.0151255

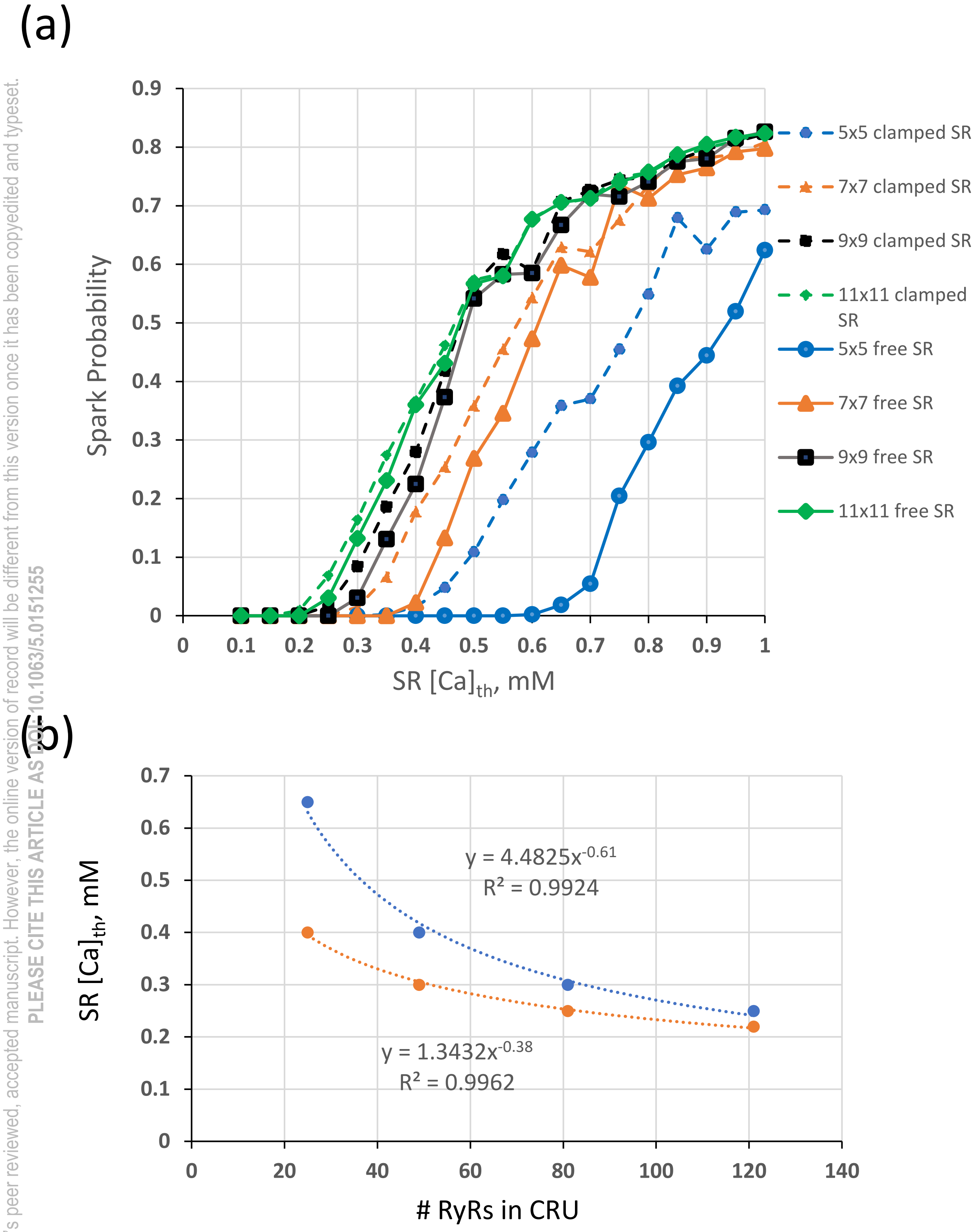

Figure 6